Boundary-layer model of pattern formation in solidification

E. Ben-Jacob, Nigel Goldenfeld, J. S. Langer, and Gerd Schön
Institute for Theoretical Physics, University of California, Santa Barbara, California 93106
(Received 20 July 1983)

We propose and investigate the properties of a model of pattern formation in crystal growth. The principal dynamical variables in this model are the curvature of the solidification front and the thickness (or heat content) of a thermal boundary layer, both taken to be functions of position along the interface. This model is mathematically much more tractable than the realistic, fully nonlocal version of the free-boundary problem, and still recaptures many of the features that seem essential for studying dendritic behavior, for example. In this paper we describe analytic properties of the model. Preliminary numerical solutions produce snowflakelike patterns similar to those seen in nature.

I. INTRODUCTION

The search for an understanding of nonequilibrium pattern-forming mechanisms, for example, dendritic solidification,[1,2] has been impeded by a lack of tractable mathematical models. The full free-boundary problem, even for the simplest case of solidification of a pure substance, has proved to be extremely difficult for either analytic or direct numerical investigation.[3] Moreover, recent studies of some overly simple one-dimensional models have made it seem likely that a correct explanation of pattern formation may be mathematically more subtle than had previously been expected.[4–6] The present investigation is an attempt to use some clues obtained in recent analyses as a guide to constructing a more useful mathematical description of solidification patterns.

The principal simplifying feature of the relatively tractable one-dimensional models is that they can be described by partial differential equations of the form

$$\frac{\partial F}{\partial t}=\Lambda\left[F,\frac{\partial^2 F}{\partial s^2},\frac{\partial^4 F}{\partial s^4}\right]. \tag{1.1}$$

Here t and s are time and linear positions, respectively; $F(s,t)$ is some displacement, for example, the position of a solidification front; and Λ is a nonlinear function of its arguments. In contrast to (1.1), a realistic solidification front is a surface, embedded in a two- or three-dimensional space, whose motion is determined by nonlocal retarded interactions. That is, the motion of a point on the front is determined by the thermal field near that point which, in turn, is determined by the latent heat which has been generated at earlier times at neighboring points. Our problem is to see how this realistic nonlocal problem might be reduced in its essential features to a simpler local model of the kind that can be described by a differential equation such as (1.1).

The idea to be developed in this paper has its roots in some of the earliest attempts to solve solidification problems.[7] The latent heat generated by a solidification front as it advances into an undercooled melt may be visualized as forming a thermal boundary layer in the liquid just ahead of the solid. The motion is governed by the rate at which the latent heat that is added to the layer on the solid side can be diffused away into the liquid. If this layer was thin everywhere compared to the radius of curvature of the solid surface, then a local approximation to the solidification kinetics, using differential rather than integral equations, might make sense. Unfortunately, most solidification phenomena seem to occur in the opposite limit. The radius of curvature at the tip of a free dendrite, for example, is generally smaller than the characteristic scale of the thermal diffusion field by an order of magnitude or more; thus the boundary-layer approximation has not seemed to be very interesting.

The main reason for reviving the idea at this time is the need for tractable mathematics; the boundary-layer approximation should bring us at least one step closer to real solidification problems than we were when dealing with the purely artificial models summarized by (1.1). As we shall see, however, the approximation may turn out to be closer to reality than expected. In the first place, the boundary layer may indeed be thin compared to the dendritic tip radius at large undercoolings; thus the model may be realistic in one physically sensible, albeit experimentally difficult, limit. It may even be possible to apply the model to the more usual case of small undercoolings by phenomenological reinterpretation of one or more system parameters, most probably the undercooling itself. But this is a speculation that is best left until later.

At this point, there are two directions which one might take. The first is to adopt a purely phenomenological approach, that is, to use the boundary-layer approximation only as a rationale for studying simple local models of interface motion. For example, consider the two-dimensional situation illustrated in Fig. 1. The liquid-solid interface is a curve which can be specified by giving its curvature K as a function of arc length S,

$$K(S,t)=-\frac{\partial\theta}{\partial S}. \tag{1.2}$$

Here, θ is the angle between the normal to the curve and some arbitrarily fixed direction in the plane. The simplest

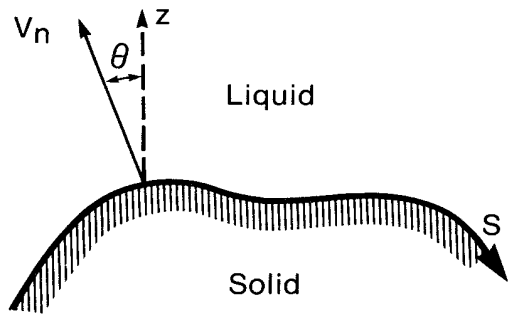

FIG. 1. Schematic illustration of a solidification front, showing various quantities defined in the text.

models that are consistent with rotational and reflection symmetries are those for which the normal growth velocity V_n is a function only of K and its even derivatives $\partial^2 K/\partial S^2$, etc. This kind of model can be described by a nonlinear partial differential equation for K as a function of S and t by writing

$$\left[\frac{dK}{dt}\right]_n = -\left[\frac{\partial^2}{\partial S^2}+K^2\right] V_n\left[K, \frac{\partial^2 K}{\partial S^2}, \ldots\right], \tag{1.3}$$

where the symbol $(d/dt)_n$ denotes the rate of change along the normal growth direction. Note that (1.3) has a structure similar to that of (1.1). This class of models may be interesting, but our preliminary investigations[8] indicate that simple choices of V_n do not reproduce the qualitative features of dendritic growth. Work along these lines is being pursued by others[9,10] at present and will not be discussed further here.

The second direction, and the one that we shall take here, is to use the boundary-layer approximation as the basis for a systematic derivation of equations of motion similar to (1.3). We shall see that this approach leads us to introduce, in addition to $K(S,t)$, a second field $H(S,t)$ which can be interpreted as the heat content of the boundary layer. The second field, with its own new equation of motion, complicates the analysis in comparison with (1.3). However, this approach has the advantage that the results can be compared directly with known special solutions of realistic solidification problems.

The main part of this paper is devoted to the above kind of comparison. The basic boundary-layer model is derived in Sec. II. Sections III and IV are devoted to relatively simple planar, circular, and spherical examples where exact realistic solutions are known both for steady-state and for some stability problems. The more interesting prelude to the dendrite, the so-called "needle-crystal" problem, is discussed in Sec. V. Some preliminary numerical results are described in Sec. VI.

II. EQUATIONS OF MOTION FOR THE BOUNDARY LAYER

Consider a purely thermal solidification problem in which a solid is growing into a uniformly undercooled melt. We shall ignore diffusion in the solid, which can have dynamical effects which are quantitatively but not qualitatively important; thus, the model we shall develop resembles the purely chemical case. The thermal picture seems more physically intuitive, however; and realistic chemical models have unpleasant complications of their own. The dimensionless temperature field u is measured from the growing solid, and is expressed in units of the ratio of the latent heat to the specific heat. The problem requires solving the diffusion equation for u everywhere in the liquid subject to two boundary conditions at the solidification front. These are, first, the Gibbs-Thomson condition,

$$u_{\text{surface}} \equiv u_s = \Delta - d_0 K\ , \tag{2.1}$$

where Δ is the dimensionless undercooling and d_0 is a capillary length proportional to surface tension. For a two-dimensional system, K is the curvature defined in (1.2); in three dimensions K is twice the mean curvature. The second boundary condition is the statement of heat conservation at the surface,

$$V_n = -D(\vec{\nabla}_n u)_s\ , \tag{2.2}$$

where D is the diffusion constant and $\vec{\nabla}_n$ is the normal gradient. The left-hand side of (2.2), in our dimensionless thermal units, is the rate at which latent heat is generated at the surface, and the right-hand side is the rate at which that heat flows into the liquid.

The crux of our approximation is the idea that, instead of solving for the exact diffusion field u, we might more simply characterize this field by the effective thickness l of the thermal boundary layer at each point along the solidification front. The situation is shown schematically in Fig. 2, where u is plotted as a function of z, the distance away from the surface along the local normal. A slightly more convenient variable is H

$$H = \int_0^\infty u\, dz \cong \alpha u_s l\ , \tag{2.3}$$

which is the heat content per unit length (or area) of the surface. Here α is a constant of order unity which we can treat for the moment as an adjustable parameter. The length l has been defined in Fig. 2 so that (2.2) becomes

$$V_n = \frac{Du_s}{l} = \frac{D\alpha u_s^2}{H}\ . \tag{2.4}$$

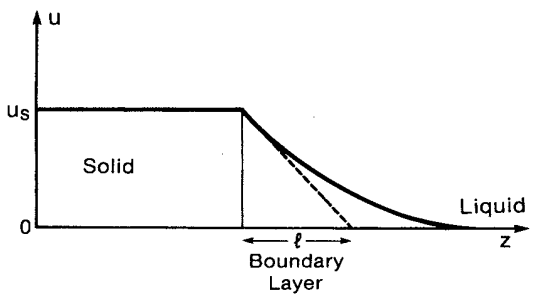

FIG. 2. Temperature vs z, the distance from the interface along the local normal.

We now must derive an equation of motion for H. This is done by looking at the thermal balance in the boundary layer as a whole. Consider the heat content $H\,\Delta S$ in a length (area) ΔS of the boundary layer. In the case $Kl \ll 1$, the time derivative of this quantity can be written in the form

$$\left[\frac{d}{dt}(H\,\Delta S)\right]_n \cong (\Delta S)V_n(1-u_s)+\alpha(\Delta S)D\vec{\nabla}_S\cdot l\vec{\nabla}_S u_s \ . \tag{2.5}$$

The first term on the right-hand side of (2.5) is the rate at which latent heat is added to the boundary layer. The total rate of heat generation is V_n; but, of this, an amount $V_n u_s$ is used to heat the solidified liquid from $u=0$ to $u=u_s$. The remainder, $V_n(1-u_s)$, enters the boundary layer. The second term describes lateral heat diffusion; the symbol $\vec{\nabla}_S$ denotes a gradient along the solidification front. The temperature gradient in this term is self-explanatory, and the factor αl has been introduced as an approximation to the z integration just as in (2.3). To eliminate the factors ΔS in (2.5), note that

$$\left[\frac{d}{dt}(\Delta S)\right]_n = (\Delta S)V_n K \ . \tag{2.6}$$

(Again, K is twice the mean curvature in three dimensions.) Thus (2.5) becomes

$$\left[\frac{dH}{dt}\right]_n = V_n(1-u_s-HK)+D\vec{\nabla}_S\cdot H\vec{\nabla}_S(\ln u_s) \ . \tag{2.7}$$

Along with the Gibbs-Thomson relation for $u_s(K)$ in (2.1), this equation of motion for H and the equation for $V_n(K,H)$ in (2.4) constitute a complete specification of the boundary-layer model.

It will be convenient for most of the following analysis to use dimensionless length and time variables, s and τ,

$$s=\frac{\Delta^3 S}{d_0}, \quad \tau=\frac{\Delta^8 Dt}{d_0^2} \ . \tag{2.8}$$

Accordingly, the scaled curvature κ and heat content h are defined by

$$\kappa=\frac{d_0 K}{\Delta^3}, \quad h=\frac{\Delta^3 H}{d_0} \ , \tag{2.9}$$

and the scaled velocity v is

$$v=\frac{d_0 V}{D\Delta^5} \ . \tag{2.10}$$

In terms of these variables, the equations of motion become

$$v_n=\frac{\alpha}{h}(1-\Delta^2\kappa)^2 \tag{2.11}$$

and

$$\left[\frac{dh}{d\tau}\right]_n = v_n(1-\Delta+\Delta^3\kappa-h\kappa)-\vec{\nabla}_s\cdot\left[\frac{h}{1-\Delta^2\kappa}\vec{\nabla}_s\kappa\right] \ . \tag{2.12}$$

The dependence of s and τ on d_0 and D is compulsory; the latter are the only dimensional parameters in this problem. The powers of Δ appearing in (2.8)–(2.10) have been chosen so that Δ will disappear from (2.11) and (2.12) in situations where it becomes very small but κ remains finite. In fact, this scaling behavior is possibly an indication of a breakdown of the boundary-layer approximation in the limit of small Δ. If some Δ-independent value of v emerges from, for example, a dendrite calculation, then (2.10) predicts that observable velocities V vanish like Δ^5. This is a physically implausible result, especially because it is independent of spatial dimension. As is generally well known, and as we shall see in the next section, the small-Δ limit is where the boundary layer becomes thick and our underlying approximation becomes invalid.

III. PLANAR, CIRCULAR, AND SPHERICAL STEADY STATES

We begin a study of special cases by considering a planar solidification front as it grows, initially without deformation, into an undercooled melt. Let the displacement of this front be $\zeta_0(\tau)$, and let $h_0(\tau)$ be the heat content of the undeformed boundary layer. Then (2.11) and (2.12) become

$$\frac{d\zeta_0}{d\tau}=v_0=\frac{\alpha}{h_0} \ , \tag{3.1}$$

$$\frac{dh_0}{d\tau}=v_0(1-\Delta) \ . \tag{3.2}$$

Dividing (3.2) by (3.1) and integrating, we find

$$h_0(\tau)=h_0(0)+(1-\Delta)\zeta_0(\tau) \tag{3.3}$$

and, from (3.1),

$$h_0(0)\zeta_0(\tau)+\tfrac{1}{2}(1-\Delta)\zeta_0^2(\tau)=\alpha\tau \ . \tag{3.4}$$

As long as Δ is less than unity and h_0 is initially positive, the system will settle down after an initial transient to the square-root law characteristic of diffusion controlled growth:

$$\zeta_0(\tau)\approx\left[\frac{2\alpha\tau}{1-\Delta}\right]^{1/2}, \quad h_0(\tau)\approx[2\alpha(1-\Delta)\tau]^{1/2} \ . \tag{3.5}$$

It is useful to rewrite this result in terms of a planar Péclet number P,

$$P\equiv\frac{Z_0 V_0}{2D}=\frac{\Delta^2 v_0\zeta_0}{2}\approx\frac{\alpha}{2}\left[\frac{\Delta^2}{1-\Delta}\right], \tag{3.6}$$

where Z_0 and V_0 are the dimensional displacement and growth velocity, respectively. Note that P is the ratio of the displacement to the diffusion length $2D/V_0$. Equation (3.6) provides a convenient form for comparing the prediction of the boundary-layer model with exact results. The relevant solution of the one-dimensional diffusion problem,

$$\frac{\partial u}{\partial t}=D\frac{\partial^2 u}{\partial z^2} \ , \tag{3.7}$$

subject to the continuity condition,

$$\left.\frac{\partial u}{\partial z}\right|_{z=z_0} = -\frac{V_0}{D} , \tag{3.8}$$

is

$$u(z,t) \approx (\pi P)^{1/2} e^P \operatorname{erfc}\left[\frac{\sqrt{P} z}{Z_0(t)}\right] , \tag{3.9}$$

where

$$\operatorname{erfc}(w) = \frac{2}{\sqrt{\pi}} \int_w^\infty e^{-y^2} dy . \tag{3.10}$$

Then the thermodynamic boundary condition, $u(Z_0)=\Delta$, yields a relation between P and Δ,

$$\begin{aligned} \Delta_{\text{exact}} &= (\pi P)^{1/2} e^P \operatorname{erfc}(\sqrt{P}) \\ &\approx \begin{cases} (\pi P)^{1/2}, & P \ll 1 \\ 1 - 1/(2P) + \cdots , & P \gg 1 . \end{cases} \end{aligned} \tag{3.11}$$

This is to be compared with (3.6), for which

$$\Delta_{\text{boundary layer}} \approx \begin{cases} (2P/\alpha)^{1/2}, & P \ll 1 \\ 1 - \alpha/(2P) + \cdots , & P \gg 1 . \end{cases} \tag{3.12}$$

The choice $\alpha=1$, consistent with $u \propto \exp(-z/l)$ in (2.3), achieves exact agreement in the large-P limit. At small P, the square-root law is correct but the numerical coefficient is wrong. The general structure of the theory remains intact; that is, we could restore complete agreement by letting the parameter α be a function of Δ.

A very similar analysis can be carried out for the two-dimensional case of a growing circle of dimensionless radius $\rho_0(\tau)$. Now the curvature $\kappa = 1/\rho_0$ enters the growth law:

$$\frac{d\rho_0}{d\tau} = v_0 = \frac{\alpha}{h_0}\left[1 - \frac{\Delta^2}{\rho_0}\right]^2 . \tag{3.13}$$

Lateral diffusion does not occur, because the curvature is independent of position around the circle, and (2.12) becomes, after division by v_0,

$$\frac{dh_0}{d\rho_0} = 1 - \Delta\left[1 - \frac{\Delta^2}{\rho_0}\right] - \frac{h_0}{\rho_0} . \tag{3.14}$$

Thus

$$h_0 = \tfrac{1}{2}(1-\Delta)\rho_0 + \Delta^3 + \frac{\text{const}}{\rho_0} , \tag{3.15}$$

where the constant must be determined by initial conditions. All trajectories in the h_0,ρ_0 plane are asymptotic at large ρ_0 to the line $h_0 = \frac{1}{2}(1-\Delta)\rho_0 + \Delta^3$, and, for positive h_0, all these trajectories are traversed in the direction of increasing ρ_0. When the circle becomes much larger than its critical radius, $\rho_0 \gg \Delta^2$, we find an analogy to (3.5)

$$\rho_0 \approx 2\left[\frac{\alpha\tau}{1-\Delta}\right]^{1/2} , \quad h_0 \approx [\alpha(1-\Delta)\tau]^{1/2} . \tag{3.16}$$

The analog of (3.6) is

$$p \equiv \frac{R_0 V_0}{2D} = \frac{\Delta^2 v_0 \rho_0}{2} = \frac{\alpha\Delta^2}{1-\Delta} , \tag{3.17}$$

where R_0 is the dimensional radius and V_0 the radial growth rate.

The asymptotically exact solution of the two-dimensional, circularly symmetric diffusion problem in the limit of large R_0 was first given by Zener.[7] In our notation he finds

$$u(r,t) \approx p e^p E_1(p r^2 / R_0^2(t)) , \tag{3.18}$$

where r is the radial distance from the center of the circle and E_1 is the exponential integral

$$E_1(w) = \int_w^\infty \frac{e^{-y}}{y} dy . \tag{3.19}$$

Setting $u(R_0)=\Delta$, we now find

$$\begin{aligned} \Delta_{\text{exact}} &= p e^p E_1(p) \\ &\approx \begin{cases} p \ln(1/p), & p \ll 1 \\ 1 - 1/p, & p \gg 1 . \end{cases} \end{aligned} \tag{3.20}$$

This is to be compared with (3.17) for which

$$\Delta_{\text{boundary layer}} \approx \begin{cases} (p/\alpha)^{1/2}, & p \ll 1 \\ 1 - \alpha/p, & p \gg 1 . \end{cases} \tag{3.21}$$

The choice $\alpha=1$ again achieves exact agreement in the large-p limit. At small p, however, the power law is wrong. This discrepancy is occurring in just the situation where we should expect the boundary-layer approximation to break down, that is, in the case where the thickness of the layer D/V_0 is large compared to the radius of curvature R_0.

The three-dimensional, spherical case shows further discrepancies, especially at small p. The exact result due to Zener[7] is

$$\begin{aligned} \Delta &= \frac{2p \operatorname{erfc}(\sqrt{p})}{2\sqrt{(p/\pi)} e^{-p} + \operatorname{erfc}(\sqrt{p})} \\ &\approx \begin{cases} 2p, & p \ll 1 \\ 1 - 1/p + \cdots , & p \gg 1 \end{cases} \end{aligned} \tag{3.22}$$

whereas the solution of the boundary-layer equations, with $\kappa = 2/\rho_0$, is

$$\Delta \approx \begin{cases} (2p/3\alpha)^{1/2}, & p \ll 1 \\ 1 - 3\alpha/(2p) + \cdots , & p \gg 1 . \end{cases} \tag{3.23}$$

IV. PLANAR INSTABILITIES

An essential feature of the boundary-layer model is that it recaptures, quite accurately, the Mullins-Sekerka instability[11] which is the underlying pattern-forming mechanism in these systems. To see this, it is simplest to return to the planar situation and look at small deviations from the unperturbed solutions $\zeta_0(\tau), h_0(\tau)$ described in Eqs. (3.1) through (3.5).

We write the total forward displacement and heat content of an almost flat front in the form

$$\zeta(s,\tau)=\zeta_0(\tau)+\zeta_1(s,\tau),\quad h(s,\tau)=h_0(\tau)+h_1(s,\tau)\ , \tag{4.1}$$

where s denotes position along the front and ζ_1 and h_1 are assumed to be small. Using

$$\kappa\cong-\frac{\partial^2\zeta_1}{\partial s^2} \tag{4.2}$$

and

$$v_n\cong v_0+\frac{\partial\zeta_1}{\partial\tau}\ , \tag{4.3}$$

we find the following linear equations of motion:

$$\frac{\partial\zeta_1}{\partial\tau}=2v_0\Delta^2\frac{\partial^2\zeta_1}{\partial s^2}-\frac{v_0^2}{\alpha}h_1\ , \tag{4.4}$$

$$\frac{\partial h_1}{\partial\tau}=[\Delta^2(2-3\Delta)v_0+\alpha]\frac{\partial^2\zeta_1}{\partial s^2}+\frac{\alpha}{v_0}\frac{\partial^4\zeta_1}{\partial s^4}-(1-\Delta)\frac{v_0^2}{\alpha}h_1\ . \tag{4.5}$$

Here we have used (3.1) to eliminate h_0 in favor of v_0, but notice that v_0 is a τ-dependent quantity. If we ignore that τ dependence, assuming that it is slow in comparison with the deformation rates of interest to us, then we can perform a conventional eigenvalue analysis. Let both ζ_1 and h_1 be proportional to $\exp(iqs+\omega\tau)$. The resulting dispersion relation is

$$\frac{\omega(q)}{v_0}=-\frac{v_0}{2\alpha}(1-\Delta)-\Delta^2q^2\pm\left[\frac{v_0^2(1-\Delta)^2}{4\alpha^2}+\left[1+\frac{v_0\Delta^2}{\alpha}(1-2\Delta)\right]q^2-\left[\frac{1}{v_0}-\Delta^4\right]q^4\right]^{1/2}\ . \tag{4.6}$$

The special case of unit undercooling, $\Delta=1$, is interesting here because it allows (4.6) to be interpreted as a true stability spectrum. In that limit, the latent heat exactly balances the undercooling and, as seen in (3.1) and (3.2), the front can move at any constant speed v_0. Equation (4.6) becomes

$$\frac{\omega(q)}{v_0}=-q^2\pm|q|\left[1-\frac{v_0}{\alpha}-\left[\frac{1}{v_0}-1\right]q^2\right]^{1/2}\ . \tag{4.7}$$

This result is usefully compared, for example, with the quasistationary approximation for the analogous stability spectrum $\omega_{QS}(q)$ in the full diffusion problem [see Ref. 1, Eq. (3.14), with $\beta=0$]. In our present dimensionless variables, this is

$$\frac{\omega_{QS}(q)}{v_0}=-\tfrac{1}{2}(q^2+v_0)+\left[q^2+\frac{v_0^2}{4}\right]^{1/2}\left[1-\frac{q^2}{v_0}\right]\ . \tag{4.8}$$

These two spectra are actually quite similar throughout the interesting range of wave numbers in which instabilities occur, that is, for values of q of order $\sqrt{v_0}$ [dimensional wave numbers of order $(V_0/Dd_0)^{1/2}$]. Both functions are shown in Fig. 3 for the case $v_0=0.01$ (and $\alpha=1$). The boundary-layer spectrum has a second branch associated with out-of-phase motions of the thermal field h; but these modes are all stable. The two branches coalesce into a complex conjugate pair at large q, where $\mathrm{Re}\omega$ decreases like $-q^2$ instead of $-q^3$ as in (4.8). The latter behavior, however, is an artifact of the quasistationary approximation,[12] and the correct behavior at large q is, in fact, $-q^2$.

It is also of some interest to look at (4.6) in the limit of small Δ,

$$\frac{\omega(q)}{v_0}\approx-\frac{v_0}{2\alpha}\pm\left[\frac{v_0^2}{4\alpha^2}+q^2-\frac{q^4}{v_0}\right]^{1/2},\quad \Delta\ll1\ . \tag{4.9}$$

The range of instability is again $q<\sqrt{v_0}$. In dimensional units, however, this corresponds to wave numbers less than $(V_0\Delta/Dd_0)^{1/2}$, thus the instability is confined to longer wavelengths at smaller Δ. When Δ is less than unity, v_0 decreases as a function of time τ. One might then think of a sequence of events in which a deformation sets in at a certain q less than $\sqrt{v_0}$, v_0 then decreases to a value such that the system is stable against small deformations at the original q, and finally the system reverts to planarity via an oscillatory decay because the square root in (4.9) has become imaginary. Such a sequence probably can be made to occur in this model, and perhaps even in real experiments, by choosing initial conditions such that

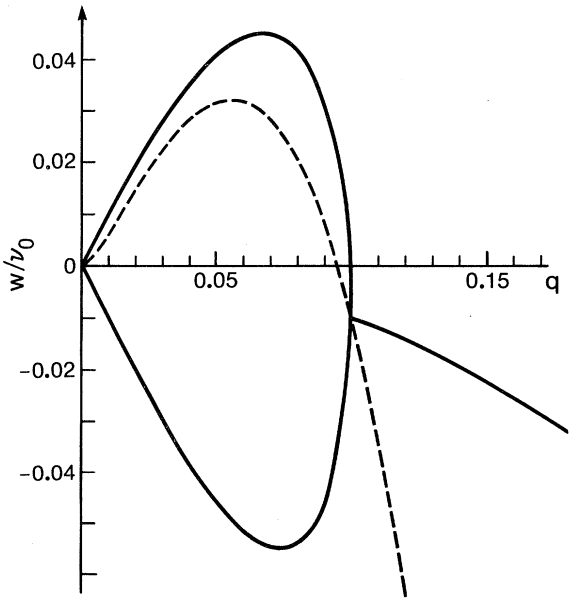

FIG. 3. Comparison between the stability spectra of the boundary-layer model (solid line) and the full diffusion problem in the quasistationary approximation (dashed line) $v_0=0.01$, $\alpha=1$.

the instability does not grow out of the range of the linear approximation before restabilization occurs. It is much more likely, however, that these instabilities will lead to qualitatively different cellular or dendritic behavior.

V. NEEDLE CRYSTALS

We turn now to the so-called "needle-crystal" problem, which has generally been considered to be an essential first step in the study of dendritic growth. We shall start by showing how the boundary-layer model recovers almost exactly the well-known family of isothermal solutions first discovered by Ivantsov.[13] The most interesting point to emerge from the following analysis is the fact that, in the boundary-layer approximation, the capillary correction to the Ivantsov model is a singular perturbation which destroys the needle-crystal solutions.

Our problem is to find shape-preserving growth forms, that is, nonplanar solidification fronts that move with constant growth velocity v in, for example, the z direction in Fig. 1. Specifically, for the two-dimensional case in which the front is described by a single curve, we look for solutions of (2.11) and (2.12) such that

$$v_n = v\cos\theta \tag{5.1}$$

and

$$\left[\frac{\partial h}{\partial \tau}\right]_\theta = 0 . \tag{5.2}$$

Note that the τ dependence in (5.2) is evaluated at constant θ so that the h field remains invariant in the frame of reference which moves at speed v. The relation between this τ derivative and the normal derivative defined following (1.3) is

$$\left[\frac{d}{d\tau}\right]_n = \left[\frac{\partial}{\partial \tau}\right]_\theta - \kappa\left[\frac{\partial v_n}{\partial \theta}\right]\frac{\partial}{\partial \theta} . \tag{5.3}$$

The relative simplicity of the boundary-layer method is apparent in the fact that we can use (2.11) and (5.1) to eliminate h from the problem, thus reducing this steady-state version of the free-boundary problem to a single nonlinear differential equation for κ as a function of θ.

The Ivantsov limit is obtained by eliminating capillary corrections proportional to d_0, that is, by setting u_s equal to Δ wherever it appears in (2.4) and (2.7). Translating this prescription into our dimensionless notation, we find

$$v_n \cong \frac{\alpha}{h} , \tag{5.4}$$

$$\left[\frac{dh}{d\tau}\right]_n \cong v_n(1-\Delta-\kappa h) . \tag{5.5}$$

The combination of (5.4) and (5.5) with (5.1)—(5.3) yields simply

$$\kappa = \frac{v}{\alpha}(1-\Delta)\cos^3\theta , \tag{5.6}$$

which is a parabola with its tip pointing in the $+z$ direction. The tip radius is $\rho = 1/\kappa(0)$; thus, in analogy to (3.6), the Péclet number p can be written in the form

$$p \equiv \frac{RV}{2D} = \frac{1}{2}\Delta^2 \rho v = \frac{\alpha\Delta^2}{2(1-\Delta)} , \tag{5.7}$$

where R and V are the dimensional tip radius and growth velocity, respectively. The exact Ivantsov result is identical to (3.11) with the planar P replaced by p. That is,

$$\Delta_{\text{exact}} \approx \begin{cases} (\pi p)^{1/2}, & p \ll 1 \\ 1 - 1/(2p) + \cdots , & p \gg 1 \end{cases} \tag{5.8}$$

which compares well with (5.7) for which

$$\Delta_{\text{boundary layer}} \approx \begin{cases} (2p/\alpha)^{1/2}, & p \ll 1 \\ 1 - \alpha/2p, & p \gg 1 . \end{cases} \tag{5.9}$$

Again, the choice $\alpha = 1$ is sensible in the large-p limit.

A similar analysis is easy to perform in three dimensions if we assume that the solidification front is a surface of revolution centered on the z axis. In this case, the curvature κ appearing in the equation of motion (5.5) must be reinterpreted as the sum of the two principal curvatures (twice the mean curvature), $\kappa_1 + \kappa_2$. Here, $\kappa_1 = -\partial\theta/\partial s$ is the curvature of the generator of the surface, and κ_2 is given by

$$\kappa_2 = \frac{|\sin\theta|}{r} , \tag{5.10}$$

where r is the radius of a circular section normal to the z axis. That is,

$$r = \left| \int_0^s \cos\theta \, ds' \right| = \left| \int_0^\theta \frac{\cos\theta' \, d\theta'}{\kappa_1(\theta')} \right| , \tag{5.11}$$

where $s = 0$ is fixed at the tip. The quantity κ appearing in the geometrical relation (5.3) is just κ_1, however. All of the above ingredients combine to yield simply

$$\kappa = \frac{v(1-\Delta)}{2\alpha}\cos^3\theta , \tag{5.12}$$

thus

$$p = \frac{\alpha\Delta^2}{1-\Delta} . \tag{5.13}$$

The exact Ivantsov formula for $\Delta(p)$ for this three-dimensional case is identical to our earlier result for the growing circle, Eq. (3.20). There is now a more serious discrepancy in the relation between Δ and p in the small-p limit; the boundary-layer approximation (5.13) predicts $\Delta \propto p^{1/2}$ whereas the exact result is $\Delta \propto p \ln(1/p)$.

Parabolic needle crystals in the Ivantsov limit seem to be about as far as one can go in finding exact analytic solutions to the full solidification problem; and it is encouraging that these solutions are recovered almost completely in the boundary-layer model. These solutions are completely unstable, however, as has been shown rigorously both for the full problem[2] and for the boundary-layer model at $d_0 = 0$.[14] Thus it is absolutely essential that capillarity be included in our equations of motion. This

brings us to the first really new result to be obtained by the boundary-layer technique: a demonstration that exact, steady-state needle-crystal solutions in this model do not survive the inclusion of capillary corrections.

For simplicity, we restrict the following analysis to the two-dimensional version of the steady-state problem in the limit of very small Δ. We also choose $\alpha=1$. That is, we look for solutions of the following set of differential equations:

$$v_n=\frac{1}{h}=v\cos\theta\ , \tag{5.14}$$

$$\left[\frac{\partial h}{\partial\tau}\right]_\theta=v_n(1-h\kappa)-\frac{\partial}{\partial s}\left[h\frac{\partial\kappa}{\partial s}\right]+\kappa\frac{\partial v_n}{\partial\theta}\frac{\partial h}{\partial\theta}=0\ . \tag{5.15}$$

Using (5.14) to eliminate v_n and h, and noting that

$$\frac{\partial}{\partial s}=-\kappa\frac{\partial}{\partial\theta}\ , \tag{5.16}$$

we find

$$\kappa=v\cos^3\theta-\frac{\kappa\cos^2\theta}{v}\frac{\partial}{\partial\theta}\left[\frac{\kappa}{\cos\theta}\frac{\partial\kappa}{\partial\theta}\right]\ . \tag{5.17}$$

Equation (5.17) has purposely been written in a form that suggests that the Ivantsov limit is the first term of an expansion of κ in powers of the dimensionless velocity v. The second term on the right-hand side of (5.17) is formally of order v^2, and the first iterations of this equation give

$$\kappa\cong v\cos^3\theta+3v^2\cos^8\theta(5\cos^2\theta-4)-9v^3\cos^{13}\theta(425\cos^2\theta-148)+\cdots\ . \tag{5.18}$$

Evaluating (5.18) at $\theta=0$, we obtain an expansion for $\kappa(0)=1/\rho$ in powers of v. This is the kind of approximation that has been used (or implied) in studies of the full problem.[15] It is clear, however, that the capillary correction is a singular perturbation, and that this expansion is, at best, asymptotic.

For an examination of the solvability of (5.17), it is useful to rewrite this partial differential equation in the form of three coupled ordinary differential equations in the independent variable s:

$$\frac{d\theta}{ds}=-\kappa\ , \tag{5.19}$$

$$\frac{d\kappa}{ds}=\lambda\ , \tag{5.20}$$

$$\frac{d\lambda}{ds}=\frac{v}{\cos\theta}(v\cos^3\theta-\kappa)+\kappa\lambda\tan\theta\ . \tag{5.21}$$

Here (5.19) is our previous expression for κ, (5.20) defines $\lambda(s)$, and (5.21) is identical to (5.17). An acceptable needle-crystal solution is a trajectory in θ,κ,λ space which starts at $s=0$ with $\theta=0$, $\lambda=0$ (by symmetry), and moves to a fixed point with $\kappa=\lambda=d\lambda/ds=0$ as s increases to infinity. From (5.21) we see that, as expected, this fixed point can occur only at $\theta=-\pi/2$. The crux of the argument is that only a single trajectory flows to this point, and that there is no symmetry or other constraint which might cause this trajectory to intersect the κ axis as is required by the starting conditions. Thus, except possibly for special values of v, there is no reason to expect needle-crystal solutions to exist.

The uniqueness of the trajectory at the fixed point can best be seen by rewriting Eqs. (5.19)—(5.21) in terms of $w=\cos\theta$, eliminating s in favor of w as the independent variable, and keeping only the leading terms near $w=0$:

$$\frac{d\kappa}{dw}=-\frac{\lambda}{\kappa(1-w^2)^{1/2}}\approx-\frac{\lambda}{\kappa}\ , \tag{5.22}$$

$$\frac{d\lambda}{dw}=\frac{v(\kappa-vw^3)}{w\kappa(1-w^2)^{1/2}}-\frac{\lambda}{w}\approx\frac{v-\lambda}{w}-\frac{v^2w^2}{\kappa}\ . \tag{5.23}$$

Rewriting (5.23) in the form

$$\kappa\approx\frac{v^2w^3}{v-\lambda-wd\lambda/dw} \tag{5.24}$$

makes it clear that $\kappa\approx vw^3$ to leading order in w; the only alternative would require that the quantity $wd\lambda/dw$ diverge, which would be inconsistent with the requirement that λ vanish at $w=0$. It remains only to show that $\kappa\approx vw^3$ defines a unique trajectory away from the fixed point. This must be true because (5.17) can be used to generate a unique expansion for κ in powers of $w=\cos\theta$,

$$\kappa=w^3\sum_{n=0}^{\infty}a_nw^n\ . \tag{5.25}$$

Inserting (5.25) into both sides of (5.17) and equating coefficients of w^n, we find a recursion relation in which the formula for a_n generated by the right-hand side of (5.17) involves only the lower order coefficients a_{n-5}, a_{n-6}, etc. Thus, all of these coefficients are unambiguously determined as functions only of v. Of course, this series is unlikely to converge at $w=1$; note the singular factors $(1-w^2)^{-1/2}$ in (5.22) and (5.23) which are related to the expected appearance of odd powers of $\sin\theta$ in the exact solution of (5.17).

Although the above analysis has been restricted to the limit of vanishingly small Δ, there seems to be no reason to expect that the qualitative nature of the result would change for arbitrary undercoolings. It also seems interesting to speculate that, if the introduction of capillarity destroys the needle-crystal solutions in the boundary-layer model, the same thing might happen in the more realistic versions of the solidification problem. We see nothing in any of the approximate solutions of this problem or in the numerical calculations of Nash and Glicksman[16] that would preclude such a possibility.

VI. PRELIMINARY NUMERICAL RESULTS

We turn now to a few comments about numerical techniques for dealing with the boundary-layer model. These remarks have to be considered in the context of the fact that, to the best of our knowledge, it has not been possible numerically to integrate the full diffusion problem far enough to see dendritic behavior. The difficulties of dealing with moving boundary problems using conventional

grid or finite element techniques stem in part from the representation and tracking of the interface, and have been discussed elsewhere.[3,17] The underlying philosophy of our approach obviates many of these difficulties at the expense, however, of introducing a new problem associated with the parametrization of the interface. At first sight, the equations of motion (1.3) and (2.7), supplemented by the relations (2.1), (2.3), and (2.4), appear to constitute a complete system of coupled partial differential equations in one space and one time dimensions. Unfortunately this is misleading because the spatial variable s itself obeys an equation of motion, Eq. (2.6), which is coupled to the remaining equations.

Suppose that we have somehow discretized (1.3) and (2.7) on a spatial grid of points $s_i(t)=s_{i-1}(t)+\Delta s_i(t)$ $(i=1,2,\ldots,N)$ taking into account the fact that Δs_i is truly a function of the label i. The time evolution of the discretized equations drives the grid points away from regions of positive curvature and toward regions of negative curvature. This tendency is undesirable not only because the computational error is unevenly distributed along the boundary, but also because of "numerical surface tension." The grid size artificially restricts the length scales probed by the dynamics, and even if there exists a natural short-wavelength cutoff in the system, the modification of the dispersion relation induced by the grid can couple to the long-wavelength behavior via the nonlinearity. In the present example this can lead to an overstabilization of the dendrite tip.

We have dealt with these difficulties by using interpolation to redistribute the grid points evenly along the boundary after each time step. Furthermore, we continuously add new grid points as the boundary expands so that the grid spacing remains constant. The most stable way that we have found is to interpolate the boundary in the space of (s,κ) rather than real space. Our time-step algorithm is a fully implicit scheme with linearization, so that the only limitation on the time step is the rate of change of the quantities we compute.

We have numerically integrated the boundary layer model for values of Δ in the range 0—1 starting from a variety of initial shapes. These include circles, ellipses, and closed curves of the parametric form (we return now to dimensionless variables):

$$\kappa(s)=a+b\cos(ms)\ . \tag{6.1}$$

In order to minimize the effects of transients we choose the initial h field such that

$$h(s,t=0)=h_0[\kappa(s)]\ , \tag{6.2}$$

where $\kappa(s)$ is given by (6.1) and $h_0(\kappa)$ is the steady-state solution (3.15) (with const=0) for a growing circle of radius $\rho_0=\kappa^{-1}$.

The limit of small Δ, although somewhat artificial, is relatively simple and will be discussed first. We have verified numerically that the interface undergoes the Mullins-Sekerka instability, the effect being most conspicuous in

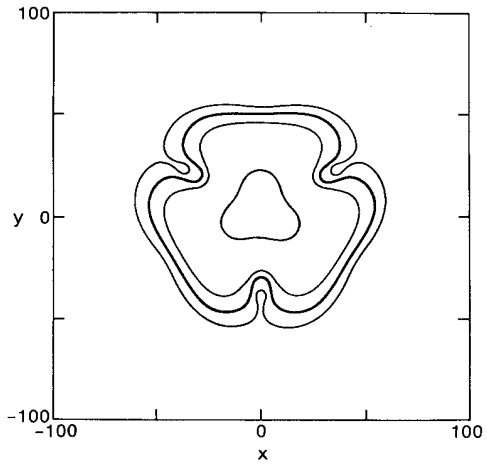

FIG. 5. Time-ordered sequence of the pattern of Fig. 2 plotted in real space, showing grooving. The thick line corresponds to the (s,κ) graph in Fig. 2.

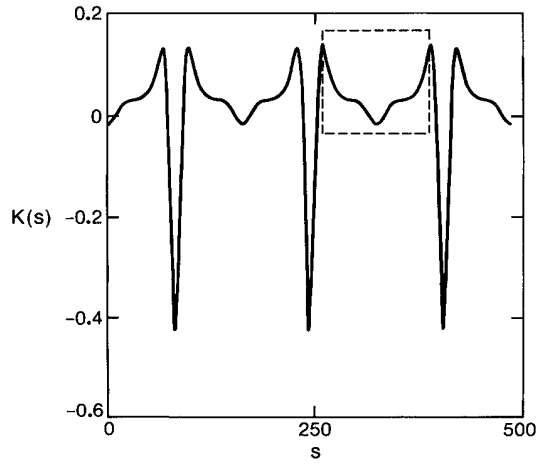

FIG. 4. κ vs s at $t=435$ in the small-Δ limit, showing the Mullins-Sekerka instability. The structure corresponds to the formation of grooves in real space.

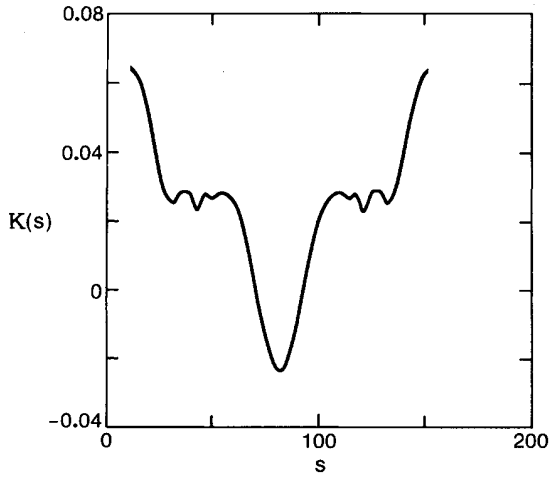

FIG. 6. Region in Fig. 4 enclosed by the dashed square at $t=520$, showing the emergence of a complex fractal-like pattern in (s,κ) space.

(s,κ) space, as shown in Fig. 4. In real space, Fig. 5, the interface develops thermal grooves which resemble those seen in undercooled crystals. Ultimately the opposite sides of the grooves intersect, but this is not important from our point of view. Correlations are absent between points close to one another in two-dimensional space, but distant along the boundary, so that the model is strictly accurate only when the groove width is much larger than the width of the boundary layer at the groove walls. As discussed in Sec. III, the small-Δ limit is not expected to be realistic. Nevertheless, the mathematical features of the small-Δ limit are related to those of the boundary layer model for $\Delta\sim 1$, and may actually be a better description of some pattern-forming system other than a dendrite. For example, a single-cell organism, *Micrasterias,* evolves by grooving in quite a similar way to the small-Δ model. The grooves create fingers which themselves become grooved at the tip, thus splitting into two fingers. If continued indefinitely, a fractal or Cayley treelike structure would form, but in practice the growth ceases as the food supply becomes exhausted. The small-Δ model continues to grow, of course, and the structure in (s,κ) space becomes increasingly complex and suggestively fractal-like. In order to follow the evolution far enough for this to become apparent, it was necessary to evolve successively smaller and smaller portions of the boundary with more and more grid points as shown in Fig. 6.

Even for $\Delta\neq 0$, the boundary does not appear to evolve toward a more dendritic structure. This is shown in Fig. 5, where the initial shape was an ellipse and $\Delta=0$. Also shown in Fig. 7 are the outer edges of the boundary layers; the dashed curves are drawn at distances $l(s)$ along the outward normals from the solidification fronts. It is clear that the growth is isotropic, and that the tip flattens, presumably because diffusion is too effective in stabilizing the boundary. We were careful to check that this result is not an artifact of our numerical scheme. What seems to be lacking in the model is a mechanism allowing instabilities to grow only in certain preferred directions as is observed experimentally. The most plausible origin of such an effect is the crystalline anisotropy. In order to verify that this could be important, we modified the boundary layer model in a simple way by allowing the factor α in (2.11) to be a function of angle θ:

$$\alpha(\theta)=\frac{1+\epsilon\cos(m\theta)}{1+\epsilon}\ , \tag{6.3}$$

where m is the crystalline symmetry. This factor inhibits growth in the nonsymmetry-related directions and thus causes the grooving instabilities to occur in those directions rather than at the dendritic tip. For $\Delta\sim 1$, this model does show dendritic behavior, with a smooth tip starting to leave a trail of side branches behind it (Fig. 8). By following the tip velocity as a function of time, we are able to check that the system is out of the initial transient stage. The behavior is particularly interesting in (s,κ) space, as shown in Fig. 9. The evolution of the dendrite appears as a periodic state modulated by an envelope function propagating away from the tip back down the dendrite. This is reminiscent of the behavior of the one-

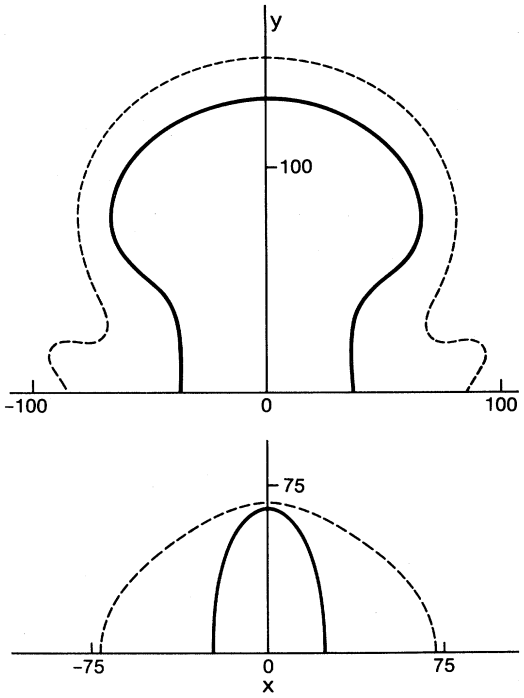

FIG. 7. Evolution of an ellipse at $t=0$ (lower diagram) until $t=100$ (upper diagram), with $\Delta=0.5$ and no anisotropy. The solid line is the interface; the dashed line is the edge of the boundary layer.

dimensional partial differential equations mentioned in the Introduction.[4–6] We have not yet succeeded in calculating the tip velocity for the boundary-layer model, so that a comparison with the marginal stability hypothesis is not presently available.

It is also interesting to compare the structures generated by the anisotropic boundary-layer model with a real snowflake. We started from a circle with a small sixfold perturbation and in addition to this symmetry, we imposed a sixfold anisotropy, with $\Delta=0.99$. In Fig. 10 we present the time development showing that many of the qualitative morphological features of a real snowflake are indeed reproduced by the anisotropic boundary-layer model. The penultimate stage shown did not evolve directly from the earlier stage (due to lack of computer time), but was inserted by hand so as to simulate an intermediate stage of growth at smaller undercooling. The final stage did, however, emerge from the preceding stage, again at $\Delta=0.99$. Although real snowflakes are not grown in two-dimensional melts at $\Delta\sim 1$, it is quite likely that the parameters in our phenomenological model, particularly Δ itself, require interpretation and are not necessarily the actual experimental values.

A more natural way to introduce crystalline anisotropy into the boundary-layer model is to modify the interfacial boundary condition (2.1) so as to include anisotropic at-

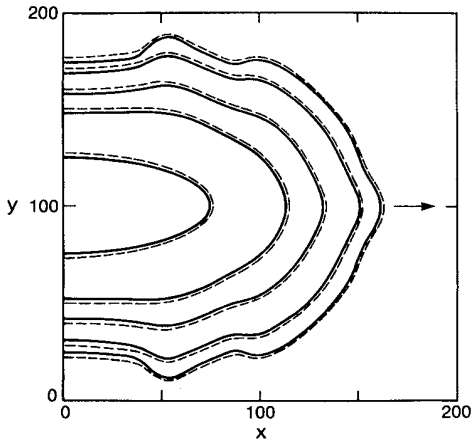

FIG. 8. Sequence of dendritelike structures with $\Delta=0.99$, $\epsilon=0.25$, and $m=4$, at times 0, 50, 75, 100, 115. The solid line is the interface; the dashed line is the edge of the boundary layer.

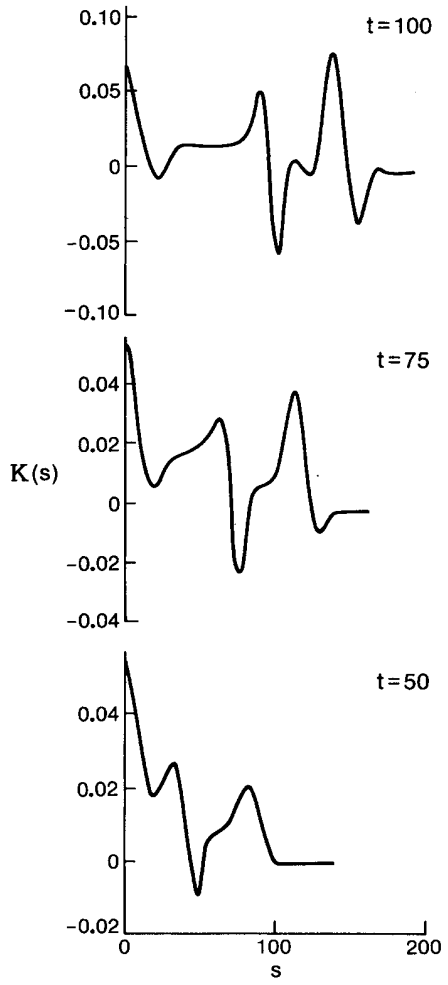

FIG. 9. Evolution of the dendritelike structure shown in Fig. 8, plotted in (s,κ) space. The tip of the dendrite is at $s=0$.

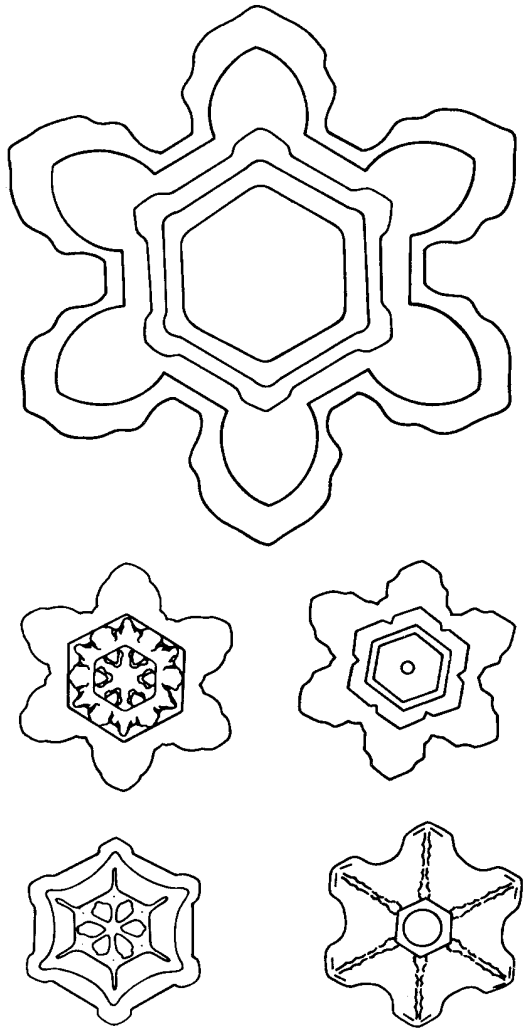

FIG. 10. Evolution of a snowflakelike structure (top) compared to sketches of real snowflakes. $\Delta=0.99$, $\epsilon=0.25$, and $m=6$. The penultimate stage did not evolve directly from the earlier stage (due to lack of computer time), but was inserted by hand.

tachment kinetics. At large undercoolings, the growth rate increases, and the assumptions of diffusion control and local equilibrium at the interface may break down. It is precisely in connection with such effects that the crystalline anisotropy is expected to play a crucial role. We can account for it, in the first approximation, by assuming that the effective temperature at the interface is reduced in an anisotropic manner. Thus we replace (2.1) by

$$u_s=\Delta-d_0K-V_n\tilde{f}(\theta)\ , \tag{6.4}$$

where

$$\tilde{f}(\theta)=\beta[1-\cos(m\theta)]\ . \tag{6.5}$$

The condition (6.4) is nothing more than the fact that above the roughening temperature, the growth velocity is

proportional to the chemical potential difference across the interface. This addition to the model is more difficult to handle numerically, but our preliminary results show similar behavior to that found with the cruder inclusion of anisotropy discussed here.

It is still not completely clear what the role of the anisotropy actually is. One possibility is that an infinitesimal anisotropy is all that is required to trigger instabilities in the preferred directions, while suppressing growth in other directions, and that the actual amplitude is not crucial. Alternatively, the amplitude of the anisotropy may need to be above some threshold in order to ensure the suppression of instabilities in the unfavored directions. Work currently in progress should be able to clarify this point.

ACKNOWLEDGMENTS

This research was supported in part by U.S. Department of Energy Contract No. DE-AM03-76SF00034 and by National Science Foundation Grant No. PHY-77-27084, supplemented by funds from the U.S. National Aeronautics and Space Administration. One of us (J.S.L.) especially acknowledges discussions with J. W. Cahn at the Institute for Mathematics and Its Applications, University of Minnesota, during a visit there.

[1]J. S. Langer, Rev. Mod. Phys. 52, 1 (1980).
[2]J. S. Langer and H. Müller-Krumbhaar, Acta Metall. 26, 1681 (1978); 26, 1689 (1978); 26, 1697 (1978).
[3]J. B. Smith, J. Comp. Phys. 39, 112 (1981).
[4]G. Dee and J. S. Langer, Phys. Rev. Lett. 50, 383 (1983).
[5]E. Ben-Jacob, H. Brand, and L. Kramer (unpublished).
[6]J. S. Langer and H. Müller-Krumbhaar, Phys. Rev. A 27, 499 (1983).
[7]For example, see C. Zener, J. Appl. Phys. 20, 950 (1949). For an early example of the use of curvature as a dynamical variable in metallurgical free-boundary problems, see W. W. Mulling, *ibid.* 27, 900 (1956); 28, 333 (1957).
[8]E. Ben-Jacob, N. D. Goldenfeld, J. S. Langer, and G. Schön (unpublished).
[9]H. Müller-Krumbhaar, Proceedings of the NATO Workshop on Chemical Instabilities, Austin, Texas, 1983 (unpublished).
[10]R. Brower, D. Kessler, J. Koplik, and H. Levine, Phys. Rev. Lett. 51, 1111 (1983).
[11]W. W. Mullins and R. F. Sekerka, J. Appl. Phys. 34, 323 (1963); 35, 444 (1964).
[12]J. S. Langer, Acta Metall. 25, 1121 (1977), especially Sec. V.
[13]G. P. Ivantsov, Dokl. Akad. Nauk SSSR 58, 567 (1947). See also G. Horvay and J. W. Cahn, Acta Metall. 9, 695 (1961).
[14]N. D. Goldenfeld and J. S. Langer (unpublished).
[15]H. Müller-Krumbhaar and J. S. Langer, Acta Metall. 29, 145 (1981); see also Ref. 2, Part 3, Appendix.
[16]G. E. Nash and M. E. Glicksman, Acta Metall. 22, 1283 (1974).
[17]Proceedings of the Conference on Fronts, Interfaces, and Patterns, Los Alamos, 1983 [Physica D (to be published)].